All fiber sensor based on Mach-Zehnder interferometer for simultaneous measurement of temperature and refractive index*

CAO Ye (曹晔), **ZHAO Chen** (赵晨)**, **and TONG Zheng-rong** (童峥嵘)
Tianjin Key Laboratory of Film Electronic and Communication Devices, School of Computer and Communication Engineering, Tianjin University of Technology, Tianjin 300384, China

(Received 14 September 2015)

In this paper, we propose and experimentally demonstrate a compact optical fiber sensor based on a Mach-Zehnder interferometer (MZI) cascaded with fiber Bragg grating (FBG) for simultaneous measurement of refractive index (RI) and temperature. In order to get a proper spectrum, we discuss the effects of different structure parameters of MZI. Using the resonant wavelength of the FBG (Dip_{FBG}) and the interference dip of the MZI (Dip1), the RI and temperature of the surrounding medium can be determined. The sensor has good operation linearity. The experimental results show that the distinctive spectral sensitivities are 0.071 75 nm/°C and −91.766 67 nm/RIU (refraction index unit) for Dip1 and 0.009 09 nm/°C for Dip_{FBG}.
Document code: A **Article ID:** 1673-1905(2015)06-0438-6
DOI 10.1007/s11801-015-5175-y

In the past several decades, optical fiber sensors based on Mach-Zehnder interferometer (MZI) have attracted great interest in manufacturing industry, environmental monitoring and bio-chemical reactions, for the advantages such as flexibility, high sensitivity and compact size over traditional sensors[1-3]. Owing to these, MZI gets a comprehensive research. And there are several methods to fabricate MZI, including core-offset structure[1,4], single-mode multimode single-mode (SMS) structure[5,6] , taper [7,8] and special fiber[9].

Recently, the MZI cascaded with fiber Bragg grating (FBG) has been popular for its high sensitivity to measure many parameters, such as temperature, refractive index (RI) and so on. In 2011, an in-fiber structure based on a hybrid fiber grating was proposed and demonstrated experimentally by Dong et al[10]. The hybrid fiber grating is formed by superimposing a short FBG on the rear part of a much longer tilted-FBG (TFBG). Its maximum RI sensitivity is 228.24 dB/RIU (refraction index unit). In 2012, Tao Qi et al[11] presented a new sensor for simultaneous measurement of strain and temperature based on core-offset inter-modal interferometer with an embedded FBG. The displacement of core-offset at both sides can affect the interference spectrum and the sensor's sensitivity. In 2013, a compact fiber sensor based on FBG embedded in a fiber modal interferometer (MI) for simultaneous measurement of strain and temperature was proposed by Zhigang Cao et al[12], where the Bragg grating is written in photosensitive fiber (PSF) and then the end of PSF is spliced to the single mode fiber (SMF) by fiber fusion splicer. The sensitivities of temperature and strain are 0.049 nm/°C and 1.09 pm/με, respectively. In 2014, Yunlong Bai et al[13] proposed and demonstrated an all-fiber sensor for simultaneous measurement of temperature and RI, which is based on a no-core fiber (NCF) and FBG. The sensitivities of temperature and RI are 0.014 nm/°C and −109.573 nm/RIU, respectively. However, a shortcoming of this sensor is that the NCF will increase the cost and make the manufacture process much more complex.

In this paper, we design and demonstrate an all-fiber sensor based on MZI cascaded with FBG. The MZI is made up of core-offset structure and spherical-shape structure. This measurement is based on the different responses of interference dips of MZI and FBG to temperature and RI. Using sensitivity matrix, we can realize the simultaneous measurement of temperature and RI.

Schematic diagrams of the experimental setup and the sensor structure are shown in Fig.1. The light from broad-band source (BBS) is launched into the sensing head, and the transmission spectrum is recorded by an optical spectrum analyzer (OSA).

An MZI can be realized by the core-offset structure and the spherical-shape structure. The input optical signal is split into the core mode and the high-order cladding modes at the core-offset structure, and then those

* This work has been supported by the National High Technology Research and Development Program of China (No.2013AA014200), the National Natural Science Foundation of China (No.11444001), and the Municipal Natural Science Foundation of Tianjin (No.14JCYBJC16500).
** E-mail: miura12@126.com

are recombined together at the spherical-shape structure. After the MZI interference, light passes through the FBG. The light which satisfies the Bragg condition can be reflected, and the rest is transmitted through the SMF. By measuring the shift of interference pattern and the Bragg wavelength of FBG from OSA, we experimentally achieve the response curves of the sensor about RI and temperature.

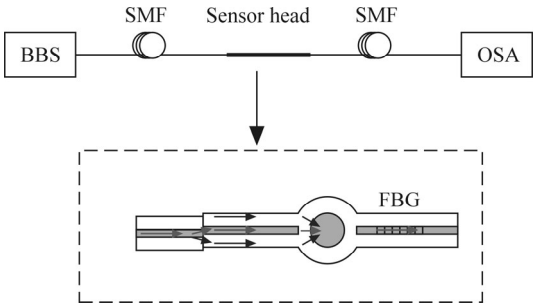

Fig.1 Schematic diagrams of the experimental setup and the sensor structure

In this paper, the spherical-shape structure is made by a commercial fusion splicer. A section of single-mode fiber is cleaved and put into the fusion splicer to make this structure. The detailed production parameters are as follows: the discharge time is 1 300 ms, and the discharge intensity is 200 bit. After the discharge, the end of the fiber becomes soft, forming a spherical-shape structure.

In a standard FBG, according to the coupled mode theory, the center-reflection wavelength of FBG is given by[14]

$$\lambda_{\mathrm{B}}=2n_{\mathrm{eff}}\Lambda\,, \tag{1}$$

where λ_{B} is the center-reflection wavelength of FBG, n_{eff} is the effective RI of the core, and Λ is the grating period.

The center-reflection wavelength of FBG (λ_{B}) is sensitive to temperature but insensitive to RI. When an ambient temperature change is applied to the FBG, the transmission dip will shift. By differentiating Eq.(1), we get

$$\frac{\Delta\lambda_{\mathrm{B}}}{\lambda_{\mathrm{B}}}=(\alpha+\xi)\Delta T\,, \tag{2}$$

where $\alpha=\frac{1}{\Lambda}\frac{\partial\Lambda}{\partial T}$ is the thermal expansion coefficient, $\xi=\frac{1}{n_{\mathrm{eff}}}\frac{\partial n_{\mathrm{eff}}}{\partial T}$ is the thermo-optic coefficient, and ΔT is the change of temperature.

Due to the phase difference between the core mode and the cladding mode, the MZI can be used to measure many environmental parameters. Here, the phase difference can be approximated as[15]

$$\Phi=\frac{2\pi\Delta n_{\mathrm{eff}}'L}{\lambda}\,, \tag{3}$$

where $\Delta n_{\mathrm{eff}}'=n_{\mathrm{eff}}^{\mathrm{co}}-n_{\mathrm{eff}}^{\mathrm{cl}}$ is the effective RI difference between the core mode and the cladding mode of the SMF, L is the interaction length between the two spherical-shape structures, and λ is the wavelength in vacuum.

When

$$\Phi=(2m+1)\pi\,, \tag{4}$$

where m is a positive integer, the wavelength values with minimum output light intensity are located at

$$\lambda_{\mathrm{Dip}}=\frac{2\Delta n_{\mathrm{eff}}'L}{2m+1}\,. \tag{5}$$

The free spectrum range (*FSR*) can be shown as

$$\Delta\lambda_{\mathrm{Dip}}=\frac{\lambda^2}{\Delta n_{\mathrm{eff}}'L}\,. \tag{6}$$

According to Eq.(5), the wavelength shift $\Delta\lambda$ caused by the variation of temperature is

$$\frac{\Delta\lambda}{\lambda_{\mathrm{Dip1}}}=\left(\frac{\xi_{\mathrm{co}}n_{\mathrm{eff}}^{\mathrm{co}}-\xi_{\mathrm{cl}}n_{\mathrm{eff}}^{\mathrm{cl}}}{n_{\mathrm{eff}}^{\mathrm{co}}-n_{\mathrm{eff}}^{\mathrm{cl}}}+\alpha\right)\Delta T\,, \tag{7}$$

where α is the coefficient of thermal expansion, ξ_{co} and ξ_{cl} are the thermo-optic coefficients of core and cladding, respectively.

From Eq.(7), we can see that with the increase of temperature, the spectrum shifts as a result of thermal expansion and thermo-optic effect. Furthermore, the wavelength shift grows linearly with the change of temperature.

The change of external RI n_{ex} causes the change of Δn_{eff}, and then leads to the shift of the interference peak. The relationship between the wavelength shift and the change of RI can be shown as

$$\frac{\Delta\lambda}{\lambda_{\mathrm{Dip1}}}=\left(\frac{1}{n_{\mathrm{eff}}^{\mathrm{co}}-n_{\mathrm{eff}}^{\mathrm{cl}}}\frac{-\partial n_{\mathrm{eff}}^{\mathrm{cl}}}{\partial n_{\mathrm{ex}}}\right)\Delta n_{\mathrm{ex}}\,. \tag{8}$$

With the change of external RI, the cladding's effective RI changes, which results in the wavelength shift. Also, there is a linear relationship between the shift and the change of RI.

It can be concluded from all the analyses above that the interference peak shift has a linear relationship with temperature and RI. There is a linear relationship between the shift of transmission peak of FBG and temperature, and it's insensitive to RI. Therefore, this kind of sensor can realize the simultaneous measurement of temperature and RI.

To get a proper transmission spectrum, we deeply research the effects of different structure parameters of MZI cascaded with an FBG. First of all, different core-offsets generate different interferences between core mode and cladding modes. Therefore, there should be a best core-offset position to obtain a clear spectrum. We get the transmission spectra with different core-offset positions as shown in Fig.2. According to Fig.2, we

know that the best offset position to get the maximum extinction ratio is 4 μm.

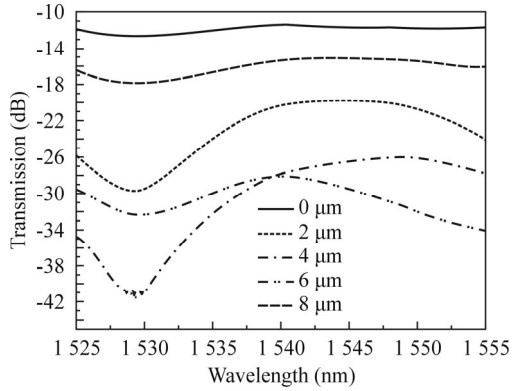

Fig.2 Transmission spectra with different offset positions

Fig.3 shows the spectra with different interference lengths. With the increase of the interference length, the spectral separation between the core-offset structure and the spherical-shape structure interference fringes decreases approximately in an inverse proportion. When the separation section is too short, it gets few interference dips and is difficult to carry out the experiments. When the long separation section generates too many dips, it also makes the experiment difficult. In addition, considering the limit of BBS with flat range of 1 525—1 560 nm, the best length between core-offset structure and spherical-shape structure is 2 cm.

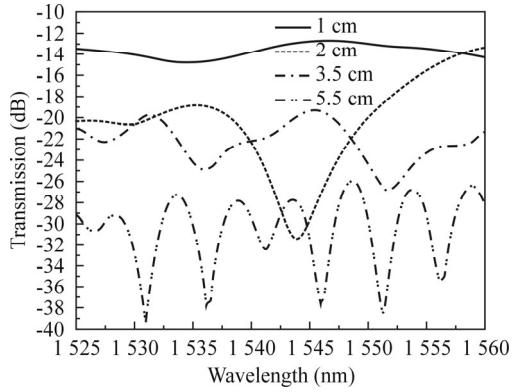

Fig.3 Transmission spectra with different interference lengths

Furthermore, we also study the sensor's characteristics with different diameters of spherical-shape structure. Fig.4 shows the images of spherical-shape structures 1–4 which are made by different discharge intensities of 140 bit, 160 bit, 180 bit and 200 bit, respectively.

The greater discharge intensity brings the greater diameter of spherical-shape structure. The increasing diameter of the spherical-shape structure makes more light in fiber cladding transmitted into the core and leads to the increase of sensitivity. The temperature and RI response characteristics are shown in Figs.5 and 6, respectively.

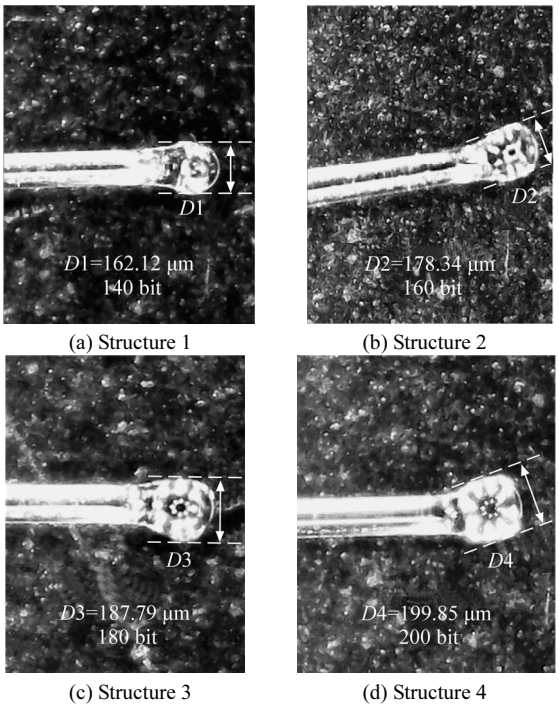

(a) Structure 1 (b) Structure 2

(c) Structure 3 (d) Structure 4

Fig.4 The images of the spherical-shape structures 1—4

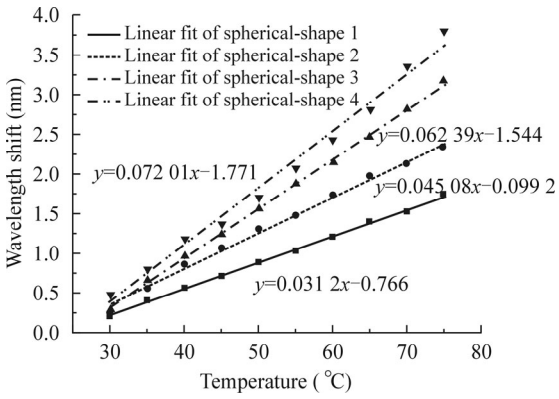

Fig.5 Temperature response characteristics with different diameters of spherical-shape structure

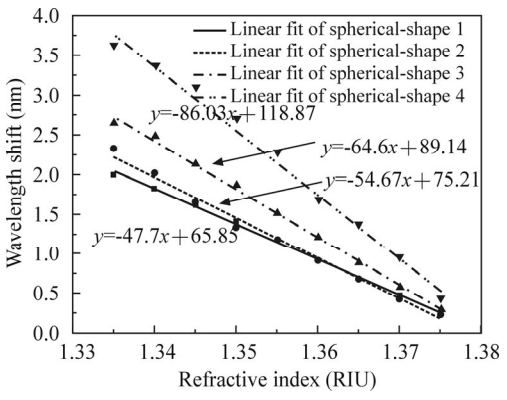

Fig.6 RI response characteristics with different diameters of spherical-shape structure

In order to study the relationship between interference length and sensor's sensitivity, we also have performed some experiments as follows. According to the analyses above, Eqs.(7) and (8) can be rewritten into another form as

$$\frac{\Delta\lambda}{\Delta T}=\alpha+\frac{2L}{2m+1}\frac{\partial\Delta n_{\text{eff}}'}{\partial T}\quad , \tag{9}$$

$$\frac{\Delta\lambda}{\Delta n_{\text{ex}}}=\frac{2L}{2m+1}\frac{-\partial n_{\text{eff}}^{\text{cl}}}{\partial n_{\text{ex}}}\ . \tag{10}$$

From Eqs.(9) and (10), with the same parameters except the interference length, the longer the interference length, the higher the sensitivity. The experimental results are shown in Figs.7 and 8. And the experimental results agree with the theoretical results very well.

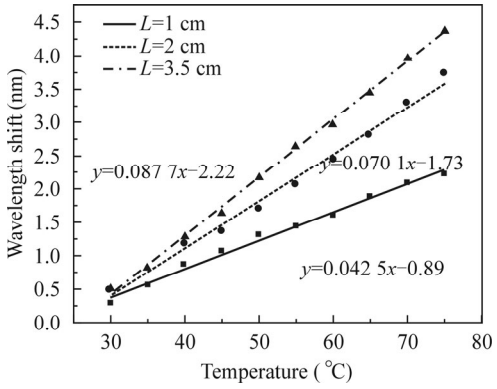

Fig.7 Temperature response characteristics with different interference lengths

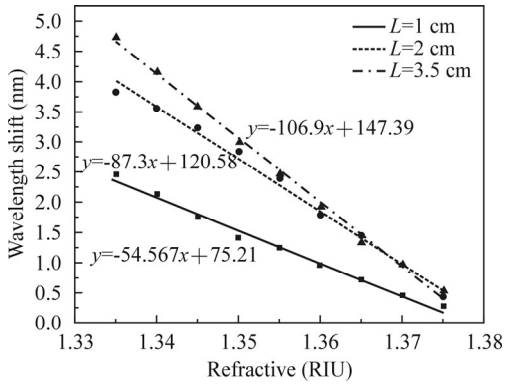

Fig.8 RI response characteristics with different interference lengths

We can increase the length between the core-offset structure and spherical-shape structure to enhance the sensor's sensitivity. This is a good way to improve the sensitivity. But the long sensor head can lead to low mechanical strength and make the experiment more difficult.

In all these experiments, standard SMF (8.3/125 μm) and FBG are used. The FBG is inscribed in SMF by femtosecond laser irradiation through a phase mask, and its reflection peak appears at 1 555.8 nm at room temperature.

To characterize the MZI response, the light from BBS is launched into SMF, and the transmission spectrum is recorded by an OSA. The attenuation spectrum of the device is obtained by subtracting the source's spectrum from the transmission spectrum of the device. Sensor head is placed straightly at room temperature, and its transmission spectrum is shown as Fig.9, where Dip1 and Dip_{FBG} represent the interference dip of the MZI and the resonant wavelength of the FBG, respectively.

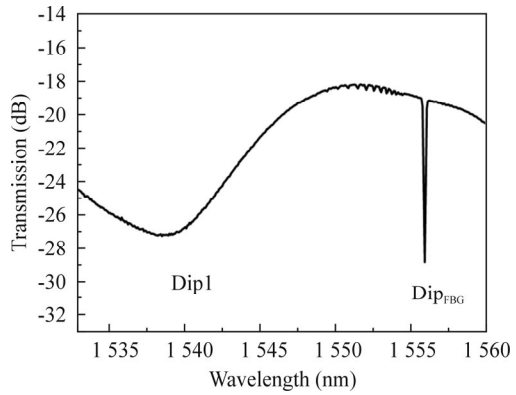

Fig.9 Transmission spectrum of the sensor at 25 °C

The temperature response characteristics are examined by placing the sensor head in the pure water with temperature range of 25—75 °C. Writing down the wavelength shifts with interval of 5 °C, the transmission spectra at 25 °C and 75 °C and the temperature response characteristic curves are shown in Fig.10. It illustrates the spectral response of the sensor to temperature. It is seen from Fig.10(b) that both Dip1 and Dip_{FBG} increase linearly with temperature. A linear fitting for the measured data gives the temperature sensitivities of 0.071 75 nm/°C for Dip1 and 0.009 09 nm/°C for Dip_{FBG}, respectively.

Then the sensor head is placed in the NaCl solutions with different concentrations at room temperature, and these solutions are used to test the RI sensitivity.

To investigate RI response characteristics, the room temperature of 25 °C is maintained, and the sensor head is sequentially immersed into a set of index matching

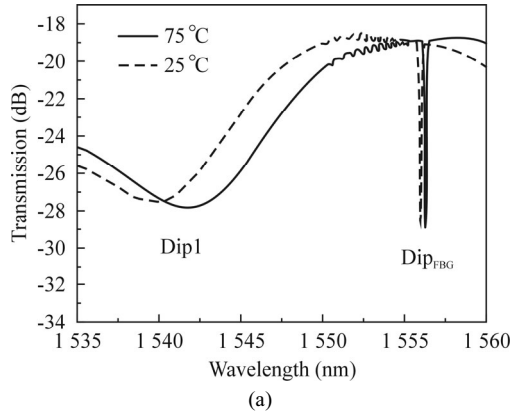

(a)

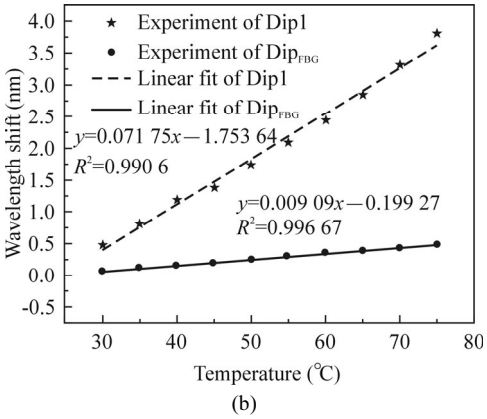

Fig.10 (a) Output transmission spectra of the sensor in pure water at 25 °C and 75 °C; (b) Temperature response characteristic curves for Dip1 and Dip$_{FBG}$

NaCl solutions ranging from 1.336 to 1.380 with a step of 0.05. The RI of NaCl solutions can be read through Abel refractometer. It can be clearly observed that the increase of the RI value leads to a blue shift of Dip1, while Dip$_{FBG}$ is essentially unchanged. Fig.11(b) shows that Dip1 is extremely sensitive to the RI change with an almost linear response, whereas Dip$_{FBG}$ remains to be a constant. The sensitivity of Dip1 is −91.766 67 nm/RIU.

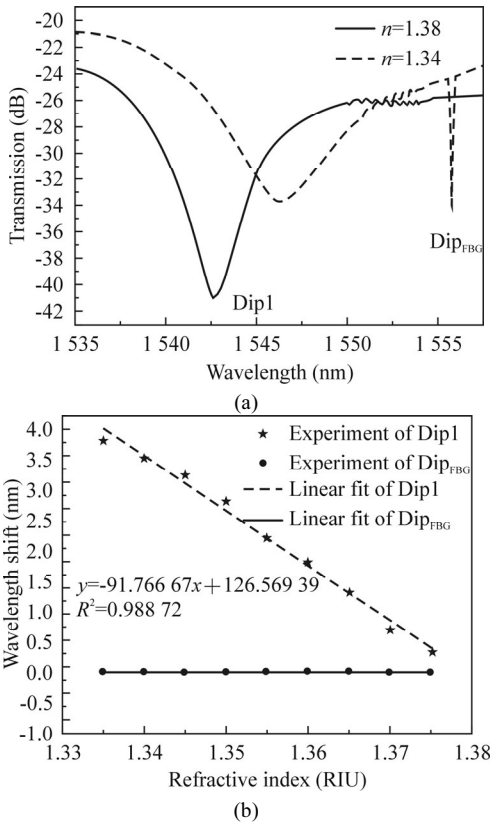

Fig.11 (a) Output spectra of the sensor in NaCl solutions with RI of 1.34 and 1.38; (b) RI response characteristic curves for Dip1 and Dip$_{FBG}$

From the experiments above, we know that Dip1 is sensitive to temperature and RI, while Dip$_{FBG}$ is only sensitive to temperature. If there are some changes in temperature (ΔT) and RI (Δn_{ex}), the wavelength shifts of Dip1 ($\Delta\lambda_1$) and Dip$_{FBG}$ ($\Delta\lambda_{FBG}$) can be described as

$$\begin{bmatrix}\Delta\lambda_1\\ \Delta\lambda_{FBG}\end{bmatrix}=\begin{bmatrix}K_{T,1} & K_{n,1}\\ K_{T,FBG} & K_{n,FBG}\end{bmatrix}\begin{bmatrix}\Delta T\\ \Delta n_{ex}\end{bmatrix}, \tag{11}$$

where $K_{T,1}$ and $K_{T,FBG}$ are temperature sensitivity coefficients of Dip1 and Dip$_{FBG}$, respectively, and $K_{n,1}$ and $K_{n,FBG}$ are RI sensitivity coefficients of Dip1 and Dip$_{FBG}$, respectively.

When RI and temperature are simultaneously applied on the sensor head, RI and temperature changes of ΔT and Δn_{ex} can be expressed by

$$\begin{bmatrix}\Delta T\\ \Delta n_{ex}\end{bmatrix}=\frac{1}{D}\begin{bmatrix}K_{n,FBG} & -K_{n,1}\\ -K_{T,FBG} & K_{T,1}\end{bmatrix}\begin{bmatrix}\Delta\lambda_1\\ \Delta\lambda_{FBG}\end{bmatrix}, \tag{12}$$

where $D= K_{T,1}\cdot K_{n,FBG} - K_{T,FBG}\cdot K_{n,1}$.

Substituting the sensitivity coefficients into the sensitivity matrix, we can get

$$\begin{bmatrix}\Delta T\\ \Delta n_{ex}\end{bmatrix}=\frac{1}{0.834\ 16}\begin{bmatrix}0 & 91.766\ 67\\ -0.009\ 09 & 0.071\ 75\end{bmatrix}\begin{bmatrix}\Delta\lambda_1\\ \Delta\lambda_{FBG}\end{bmatrix}. \tag{13}$$

As a result, when temperature and RI change simultaneously, we can easily calculate the changes of the measured parameters according to the wavelength shift and the sensitivity matrix. The sensing resolution of the sensor is limited by the wavelength resolution of the measurement equipment (i.e., OSA). When the resolution of OSA is 0.01 nm, the corresponding resolutions of temperature and RI are 1.1 °C and 0.000 9 RIU, respectively. It has proved the merits of this sensor structure.

An optical fiber sensor for simultaneous measurement of temperature and RI is proposed by using MZI cascaded with FBG. The temperature and RI experimental results both show good agreement with theoretical analyses. Experimental results show that this sensor has a linear temperature sensitivity of 0.071 75 nm/°C and an RI sensitivity of −91.766 67 nm/RIU. Transmission dip Dip$_{FBG}$, which is formed by FBG, is only sensitive to temperature, and its sensitivity is 0.009 09 nm/°C. The sensor works in transmission mode with a compact sensing element, and is a potential candidate for chemical and biological sensing applications.

References

[1] Jinping Chen, Jun Zhou and Zhenhong Jia, IEEE Photonics Technology Letters **25**, 2354 (2013).

[2] Yanzhen Tan, Li-Peng Sun, Long Jin, Jie Li and Bai-Ou Guan, IEEE Photonics Technology Letters **25**, 2201 (2013).

[3] Yang Ran, Long Jin, Yan-Nan Tan, Li-Peng Sun, Jie Li and Bai-Ou Guan, IEEE Photonics Journal **4**, 181 (2012).

[4] Jiangtao Zhou, Yiping Wang, Changrui Liao, Guolu Yin, Xi Xu, Kaiming Yang, Xiaoyong Zhong, Qiao Wang and Zhengyong Li, IEEE Photonics Technology Letters **26**, 508 (2014).

[5] Wenjun Zhou, Yan Zhou, Xinyong Dong, Liyang Shao, Jia Cheng and Jacques Albert, IEEE Photonics Journal **4**, 1051 (2012).

[6] Yuan Gong, Tian Zhao, Yun-Jiang Rao and Yu Wu, IEEE Photonics Technology Letters **23**, 1041 (2011).

[7] Jieliang Li, Weigang Zhang, Shecheng Gao, Zhiyong Bai, Li Wang, Hu Liang and Teiyi Yan, IEEE Photonics Technology Letters **26**, 1041 (2014).

[8] Tao Li, Xinyong Dong, Chi Chiu Chan, Chunliu Zhao and Peng Zu, IEEE Sensors Journal **12**, 2205 (2012).

[9] Peng Zu, Chi Chiu Chan, Wen Siang Lew, Limin Hu, Yongxing Jin, Hwi Fen Liew, Li Han Chen, Wei Chang Wong and Xinyong Dong, IEEE Photonics Journal **4**, 491 (2012).

[10] Tao Li, Xinyong Dong, C. C. Chan, Chun-Liu Zhao and Shangzhong Jin, IEEE Photonics Technology Letters **23**, 1706 (2011).

[11] Tao Qi, Shilin Xiao, Jie Shi, Zhao Zhou, Meihua Bi and Pingqing Li, Simultaneous Strain and Temperature Measurement Using Compact Core-Offset Inter-Modal Interferometer with Embedded Fiber Bragg Grating, Asia Communications and Photonics Conference, 1 (2012).

[12] Zhigang Cao, Xiaochun Ji, Rui Wang, Zhao Zhang, Tao Shui, Feng Xu and Benli Yu, IEEE Sensors Journal **13**, 1447 (2013).

[13] Yunlong Bai, Bin Yin, Chao Liu, Shuo Liu, Yudong Lian and Shuisheng Jian, IEEE Photonics Technology Letters **26**, 2193 (2014).

[14] K. O. Hill and Gerald Meltz, Journal of Lightwave Technology **15**, 1263 (1997).

[15] Zhaobing Tian, Scott S.-H. Yam, Jack Barnes, Wojtek Bock, Patricia Greig, James M. Fraser, Hans-Peter Loock and Richard D. Oleschuk, IEEE Photonics Technology Letters **20**, 626 (2008).

.